Ultrafast Detection of TeraHertz Radiation with Miniaturized Optomechanical Resonator Driven by Dielectric Driving Force

Jiawen Liu, Baptiste Chomet, Paolo Beoletto, Djamal Gacemi, Konstantinos Pantzas, Grégoire Beaudoin, Isabelle Sagnes, Angela Vasanelli, Carlo Sirtori, Yanko Todorov

ACS Photonics

pubs.acs.org/journal/apchd5

Letter

Ultrafast Detection of TeraHertz Radiation with Miniaturized Optomechanical Resonator Driven by Dielectric Driving Force

Jiawen Liu,* Baptiste Chomet, Paolo Beoletto, Djamal Gacemi, Konstantinos Pantzas, Grégoire Beaudoin, Isabelle Sagnes, Angela Vasanelli, Carlo Sirtori, and Yanko Todorov*

Cite This: https://doi.org/10.1021/acsphotonics.2c00227

Read Online

ACCESS | Metrics & More | Article Recommendations | Supporting Information

ABSTRACT: We report on an optomechanical terahertz (THz) meta-atom detector empowered by a dielectric driving force scheme. The meta-atom consists of a suspended half-wavelength THz antenna that sustains high quality factor mechanical modes. The THz radiation is resonantly absorbed by the meta-atom and enforces an optimized photothermal mechanism that produces mechanical oscillations, with a responsivity of 30 pm·nW^{-1}/3 Hz·nW^{-1} in terms of amplitude/frequency response. Moreover, in this optomechanical system, THz-induced Duffing nonlinearities can be easily observed. The dielectric driving forces allow the implementation of a frequency phase-lock loop, with a harmonic bandwidth on the order of 1 MHz, and thus, square wave THz signals can be temporally recovered at frequencies up to 100 kHz.

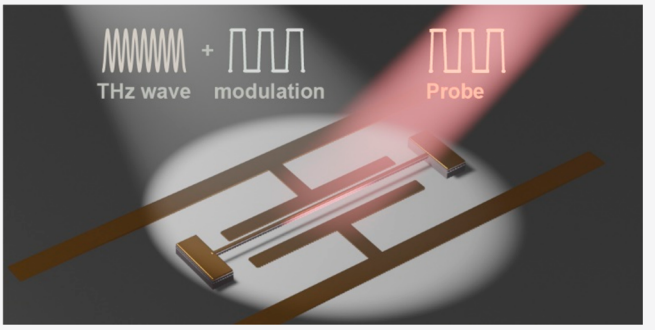

KEYWORDS: *terahertz detection, terahertz resonator, optomechanics, gradient force, phase-lock loop, Duffing nonlinearity*

In an inhomogeneous electric field, polarizable materials are attracted toward the maximum of the field strength by the dielectric gradient force. This phenomenon has been exploited in various contexts such as optical trapping of microparticles[1] or dielectrophoresis.[2] As reported by Unterreithmeier, Weig, and Kotthaus, the dielectric gradient force can become a powerful tool for driving nano/microelectromechanical systems (NEMS/MEMS),[3] which has fueled the spectacular development of cavity optomechanics in the last few decades.[4,5] Indeed, the mechanical response to gradient forces is an instantaneous effect and has no constraints in the choice of the materials, in contrast to, for example, the piezo-electrical driving scheme.[6] Here the dielectric driving scheme is combined with micro-optomechanical resonators[7,8] to implement miniaturized detectors working in the terahertz (THz) frequency domain.

Currently, THz technologies are being developed for many applications such as wireless communications,[9] imaging, and biochemical sensing.[10,11] Most of the very sensitive commercial THz detectors (Si/Ge bolometers, pyroelectric detectors, Golay cells, etc.) cannot operate at room temperature[12] and are quite slow (typically below 10 kHz), as they rely on thermal effects limited by the thermal diffusion time, τ. As τ scales inversely to the square of the size of the sensing element, it is pertinent to explore alternative approaches that take advantage of size miniaturization in order to increase the detector speed and the operating temperature. In our design, we use a half wavelength THz resonator that acts as a receiving antenna for incoming radiation. The resonator is made of a metal−semiconductor bilayer that is optimized for thermomechanical effects, which yields a mechanical response owing to the Joule heating induced by the impinging THz wave.[13] This scheme is further supplemented with microelectrodes in order to control the mechanical oscillation using the dielectric gradient force. That scheme enables frequency phase-lock loop (PLL) detection,[9] where THz radiation is thus detected without specific frequency modulation, as recently demonstrated by Hirakawa and co-workers in a piezoelectric MEMS device.[14] In the present case, owing to the size miniaturization and the compact dielectric force scheme, we achieve a harmonic bandwidth for the PLL detection on the order of 1 MHz, which is only limited by the PLL electronics.

Our micro-optomechanical device, shown in Figure 1a, is designed in a dog-bone shape, consisting of a suspended mechanical nanobeam (length l = 17 μm, width w = 250 nm, and total thickness u = 350 nm), which is doubly clamped between two anchoring pillars. The bimaterial that constitutes the beam is composed of a gold layer (thickness u_{Au} = 150 nm) deposited on top of GaAs (u_{GaAs} = 200 nm). The dimensions of the dog-bone shape have been carefully chosen so that the structure acts

Received: February 9, 2022

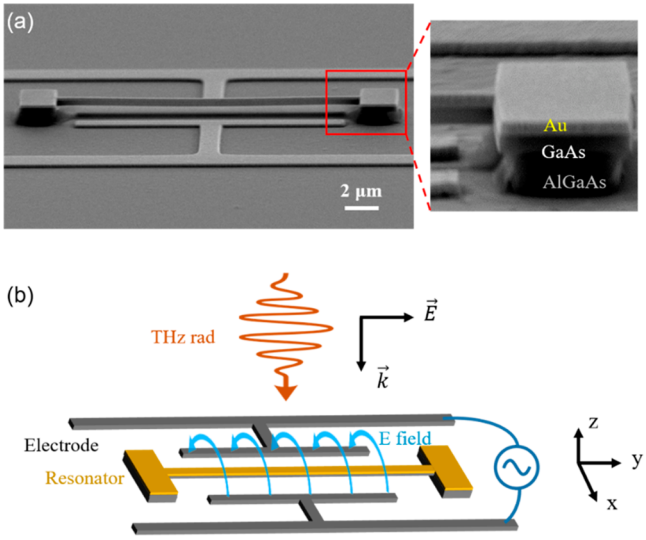

Figure 1. (a) Scanning electron microscope (SEM) image of a fully processed bimaterial optomechanical resonator consisting of a suspended beam (length l = 17 μm, width w = 250 nm, and total thickness u = 350 nm), two anchoring pillars, and microelectrodes. Zoom-in image: bimaterial structure composed of 150 nm Au and 200 nm GaAs, attached to the substrate by a sacrificial layer (500 nm AlGaAs). (b) Schematic of the optomechanical system, with indications of the RF voltage and THz radiation.

as a half-wavelength THz resonator matching the wavelength of our radiation source, a 2.5 THz (λ = 120 μm) quantum cascade laser (QCL).[15] The excitation of the THz resonator by the external source induces eddy currents that heat up the mechanical nanobeam and generate thermal strains due to the different thermal expansion coefficients of the gold and GaAs. As a result, our devices strongly respond to the incident THz radiation, showing changes in the vibration amplitude, frequency, and phase and thus can be employed for the detection of THz waves.

In order to implement the dielectric driving force, we design and fabricate microelectrodes on both sides of the mechanical beam, with a separation distance of about 2 μm (Figure 1b). These microelectrodes will be used to drive the motion of the beam to set up the phase-lock loop for fast THz detection with no need for specific modulation frequencies, as will be discussed later. Details on device fabrication have been provided in the Supporting Information (SI).

A home-built microscope is employed to measure the vibration modes of individual devices through an optical read-out method (see the schematic of the setup in ref 7). These measurements reveal a mechanical oscillation at 3.17 MHz at ambient pressure, which corresponds to the fundamental out-of-plane flexural mode. The quality factor of this mechanical mode is about $Q \sim 700$, measured in a low-pressure environment of 1 mbar. The THz response of the dog-bone resonator has been probed by THz time-domain spectroscopy (TDS) measurements, which confirms that the resonance frequency of the fabricated device agrees well with our design. Further details on the optical and mechanical characterizations of the structure as well as on the calibration of the mechanical displacements[16] are provided in the SI (sections C and D).

As a first step, we characterize the mechanical response under THz illumination (see SI, section A).[7,8,17] In the present case, such measurements allow us to confirm the origin of the thermomechanical effect. For this purpose, the driving current of the QCL is radio frequency (RF) modulated at a frequency close to the mechanical mode f_m of the nanobeam. The resulting THz intensity modulation induces a mechanical oscillation, visible as a sharp peak in the RF spectra of Figure 2, where the results for

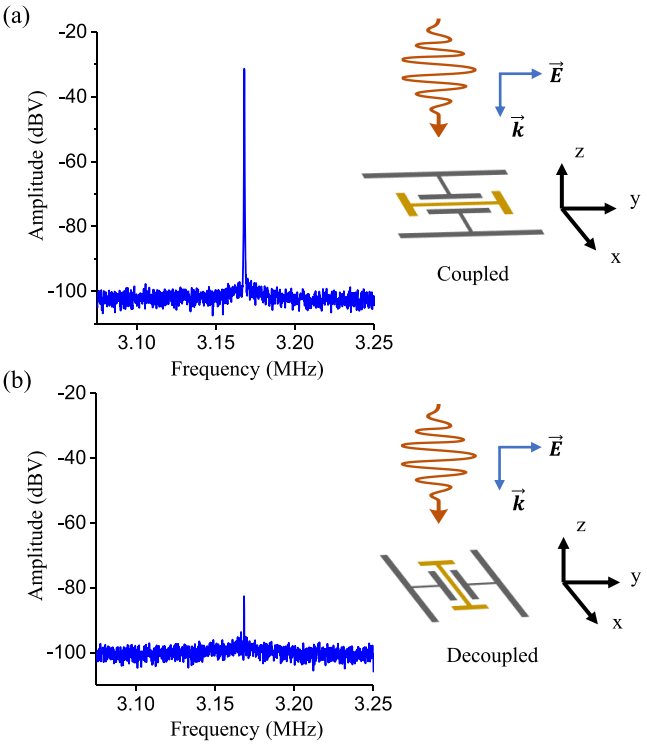

Figure 2. Polarization-dependent responses. The THz wave propagates along the z axis and polarizes along the y axis. The orientation of the resonator is along the y (a) or x (b) axes to couple or decouple to the incident THz waves, resulting in a 60 or 12 dB detected signal, respectively.

two cross-polarizations are shown. There are two possible reasons for the thermal force generated on the bimaterial beam: (1) the heat generated in the thin part of the dog-bone owe to the eddy current induced by the resonant absorption of the THz signal and (2) the heat generation in the substrate beneath the structure, which then diffuses into the beam through the anchoring pillars. Both mechanisms feature similar thermal diffusion times $\tau \propto l^2$ obeying Fick's law of diffusion.[18] To evaluate the weight of these two contributions, we study the dependence of the resonant THz absorption in the meta-atom as a function of the polarization of the incident THz wave. Indeed, only the electric field along the dog-bone is absorbed, while the substrate heating occurs independently on the particular polarization of the incident wave. Figure 2a reports the results for an electric field parallel to the mechanical beam with a signal level that is 60 dB above the Brownian motion noise, while in Figure 2b, for an electric field orthogonal to the dog-bone, the THz signal becomes much weaker and rises only 12 dB above the noise. This proves that more than 99% of the thermal forces result from the resonantly induced eddy currents.

The optomechanical responsivity of the device has been characterized by measuring the mechanical RF spectra as a function of the incident THz power (Figure 3a). For a harmonic modulation, the output power from the QCL can be expressed as $P_{QCL} = \frac{P_0}{2}[1 + \cos(\omega_{mod}t)]$, where $P_0 \sim 1.2$ mW is the peak

https://doi.org/10.1021/acsphotonics.2c00227
ACS Photonics XXXX, XXX, XXX−XXX

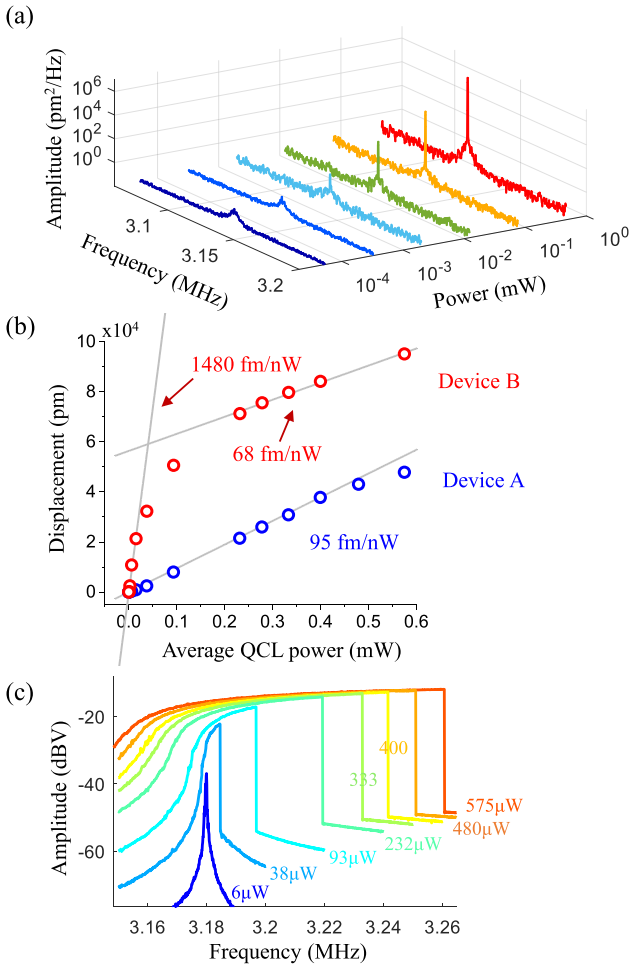

Figure 3. (a) Mechanical RF spectra measured with various incident QCL power. Resolution bandwidth: 100 Hz. (b) THz-induced displacement as a function of the average QCL power. Blue dots: device A. Red dots: device B. The slopes refer to the external optomechanical responsivity of the system. (c) Amplitude responses of the device B when sweeping the modulation frequency of the QCL with various power. At low power, the response is in the linear regime with a Lorentzian line shape (blue curve). For high powers, we observe the typical response of a Duffing oscillator.

power and ω_{mod} is the modulation frequency. Power $\frac{P_0}{2}$ can be attenuated with paper filters down to ∼50 nW, for which the minimal detectable displacement, ∼5 pm, becomes comparable with the Brownian noise. In Figure 3b (blue dots) we report the amplitude of the mechanical oscillations as a function of the QCL power. The dependence stays linear for a wide range for the average QCL power, from 0 to the maximum value ($\frac{P_0}{2} = 0.6$ mW), with a slope of ∼95 fm/nW.

Stronger responses (red dots in Figure 3b) have been observed on another sample with a higher mechanical quality factor ($Q \sim 8000$ at 1 mbar). For low QCL powers ($P_0 < 0.1$ mW), the displacement amplitude increases 15× faster with the QCL power than the previous device, with a slope of 1480 fm/nW. Notably, this device can be easily driven into the nonlinear oscillation regime by the incident THz radiation. A typical Duffing response, which corresponds to a cubic nonlinearity,[19] is obtained (Figure 3c) when sweeping the modulation frequency of the QCL and recording the amplitude. The Duffing regime is responsible for the saturation of the amplitude response visible in Figure 3b. Systematic investigation of the nonlinear regime will be reported elsewhere. In the following, we designate this sample as device B and the former sample as device A.

The slope between the displacement and the radiation power refers to the external responsivity of the device, which is defined with respect to the total modulated power P_{QCL} delivered by the QCL. In the present devices, we can estimate the actual THz power, P_{abs}, dissipated into a single meta-device so that to estimate the internal responsivity. By considering the model (see SI, section E) for a thermal diffusion along the nanobeam, P_{abs} is related to the temperature rise ΔT in the device through the formula $P_{abs} = \frac{6uw\lambda_T}{l}\Delta T$, where $\lambda_T \sim 163$ $Wm^{-1}K^{-1}$ is the average thermal conductivity of the bilayer beam. We consider a static situation where the incident QCL power is not modulated (continuous wave, CW). The temperature rise, ΔT, can be determined experimentally from the frequency shift, Δf, of the mechanical resonance that is induced by the thermal strain.[20] The link is provided by the formula $\Delta T = \frac{1}{C_T}\frac{\Delta f}{f_0}$, where f_0 is the initial resonance frequency of the mechanical beam without THz radiation, C_T (∼0.005/K, see SI, section F) is the temperature−frequency coefficient[20] that depends on the geometry of the beam. For device A, we observe that the CW QCL power $P_{QCL} \sim 1.2$ mW induces a frequency shift $\Delta f = f(300\ K) - f(300\ K + \Delta T) = 12$ kHz (Figure 4a,c), corresponding to a temperature change $\Delta T \sim 0.77$ K. The corresponding absorbed power is thus $P_{abs} \sim 3.8$ μW, which yields a coupling efficiency for a single device $P_{abs}/P_{QCL} \sim 0.3\%$ (comparable to the result in ref 8) and an internal responsivity ∼30 pm/nW. It is interesting to note that such a measurement provides an experimental tool to access directly the electromagnetic power dissipated into a single meta-atom resonator with strong subwavelength dimensions.

The THz radiation-induced frequency shift indicates that our device can also function as a miniaturized bolometer, such as the ones described in refs 14 and 21. The minimum detectable power corresponds to the minimum resolvable frequency shift Δf_{HWHM}, that is, the half-width at half-maximum of the resonance peak. To evaluate the potential of our devices working as bolometers, in this experiment we consider device B, with the narrowest mechanical line width $f_{HWHM} \sim 200$ Hz. As a result, the resolvable temperature rise induced by the THz illumination is $\Delta T_{res} = \frac{1}{C_T}\frac{\Delta f_{HWHM}}{f_0} \sim 12$ mK, which leads to a minimum detectable power $P_{res} = \frac{6uw\lambda_T}{l}\Delta T_{res} \sim 60$ nW. As shown in Figure 4b, when measured under different QCL powers, P_{QCL} from 0 to ∼1.2 mW, the maximal shift Δf is 25 kHz, corresponding to an absorbed power $P_{abs} \sim 7.9$ μW. Therefore, the coupling efficiency for device B is $P_{abs}/P_{QCL} \sim 0.66\%$. Figure 4d shows the linear dependence between the frequency shift and the QCL power, with an external responsivity $R = \frac{\Delta f}{P_{QCL}} \sim 21$ kHz/mW. Considering the coupling efficiency of 0.66%, the internal responsivity is thus estimated to be $R \sim 3$ Hz/nW. This performance is comparable to the recently reported MEMS bolometer in ref 22, whose responsivity is already enhanced by 2 orders of magnitude through the internal mode coupling. In comparison, the devices reported here are more compact and prone to large area integration; furthermore, their performance can be further enhanced by improving the collection efficiency through coupling with an additional antenna element.[23]

https://doi.org/10.1021/acsphotonics.2c00227
ACS Photonics XXXX, XXX, XXX−XXX

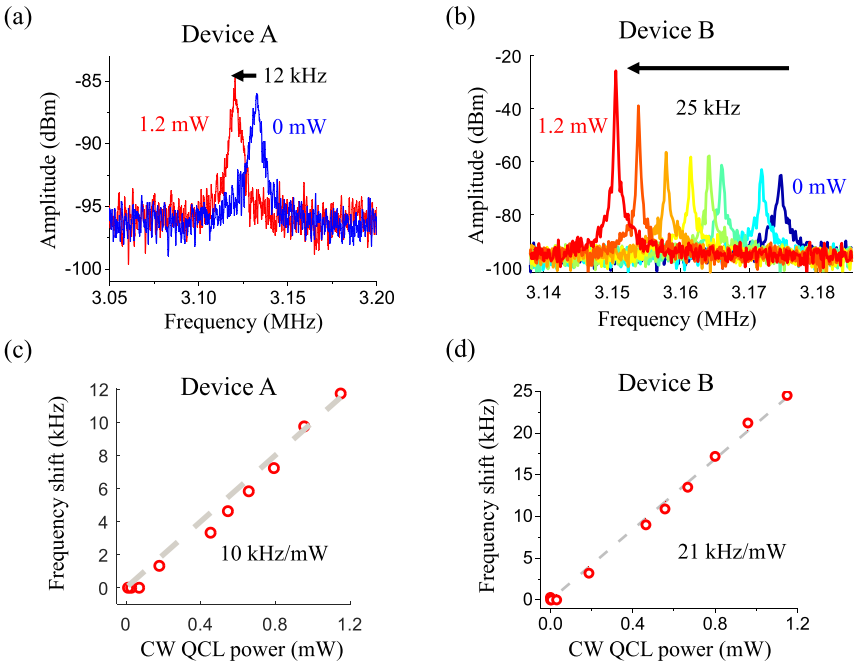

Figure 4. Photothermally induced frequency shifts of the mechanical resonance in the case of the device A (a) or device B (b). (c, d) Frequency shifts as a function of the incident continuous wave (CW) QCL power. All spectra corresponding to the experimental points in (c) are provided in the SI.

The linear dependence of the frequency shift on the THz power can be exploited to implement a phase-lock loop (PLL). The counteraction of the loop is established here by using the dielectric driving scheme. Driving voltage on the microelectrodes sets the beam oscillation, and the PLL is used to stabilize its vibrational frequency to a value f_m. The shift Δf_m, induced by the incident THz power, is detected by the PLL and converted into an output signal.

Studies were performed on device A. A 1.5 V RF voltage is applied to the microelectrodes, and the dielectric force loaded on the nanobeam is estimated to be ∼7 pN (see SI, section G). We sweep the modulation frequency of the QCL over a wide range, from 3 kHz to 8 MHz, and record the amplitude of the output signal, as shown in Figure 5a (orange curve). The amplitude remains constant (frequency shift $f_m \sim 1.8$ kHz) until the modulation frequency of the QCL approaches the cutoff of the PLL (∼1 MHz), indicating that the detection speed of the system is limited by PLL's transfer bandwidth (black curve). The intrinsic limit of this type of detection is set by a thermal diffusion time on the nanobeam, which is estimated to be τ_D = 1.2 μs in our case (see SI, section H). The corresponding detection bandwidth $1/\tau_D$ is thus very comparable to the PLL cutoff. A similar result is obtained on another representative device, and further power dependent measurements confirm a linear dependence between the frequency shift and QCL irradiation power (SI, section I). In addition, Figure 5a also shows that the minimum resolvable frequency shift, limited by the pickup signal from the PLL electronics (gray curve), is on the order of 1 Hz, much lower than the mechanical resonance line width (∼4 kHz in Figure 4a) of this device. Given the frequency shift of 1.8 kHz measured with 0.5 mW QCL power and the linear frequency-power dependence, the minimum detectable THz radiation through this method is then estimated to be ∼280 nW.

To further characterize the response speed of our device, we also use it to temporally recover the input square pulses with various repetition frequencies. In Figure 5b, the output signals (blue curves) are observed by an oscilloscope together with the THz input signals (red curves). We start with a low frequency at 1 kHz, as shown in the top panel, and the output signal recovers a square shape. As the frequency increases, the output signal starts to deform at 10 kHz and changes to triangular shapes at 100 kHz. The signal then becomes sinusoidal for frequencies up to 350 kHz, indicating that the highest Fourier harmonics are strongly attenuated. Therefore, by probing our system with square pulses, we show that the input THz signal can be well recovered at a frequency of 100 kHz, this speed is 20× faster than the recent report of a MEMS THz detector,[14] thanks to its shorter thermal diffusion time resulting from the miniaturized structure.

In summary, we have presented miniaturized optomechanical devices that sensitively detect THz radiation at room temperature with a responsivity of ∼30 pm/nW (or 3 Hz/nW) in terms of the amplitude (or frequency) response. A phase-lock loop is established for single meta-devices by the dielectric driving scheme, which allows THz detection with a harmonic bandwidth on the order of 1 MHz, and temporal reconstruction of the THz signal with a repetition rate up to 100 kHz. Therefore, our device can serve as a fast, sensitive THz detector to enable many applications such as THz imaging. It is also feasible to scale down our dog-bone design to implement optomechanical detectors working at other frequency ranges such as the mid-infrared.[24] The strong THz responses of the devices result from the thermomechanical effect in the bimaterial structure, which allows the demonstration of the nonlinear Duffing behavior under the driving by the THz radiation. Furthermore, strong RF bias also allows driving the beam to the strongly nonlinear regime. This opens a new possibility for THz sensing, possibly taking advantage of nonlinear interactions[25,26] between the THz and RF driving modes. A compelling perspective is to exploit the squeezing of the thermal noise that can be observed in such regimes.[27,28] The universality of the dielectric driving scheme can also be implemented in other semiconductor materials, such as

https://doi.org/10.1021/acsphotonics.2c00227
ACS Photonics XXXX, XXX, XXX−XXX

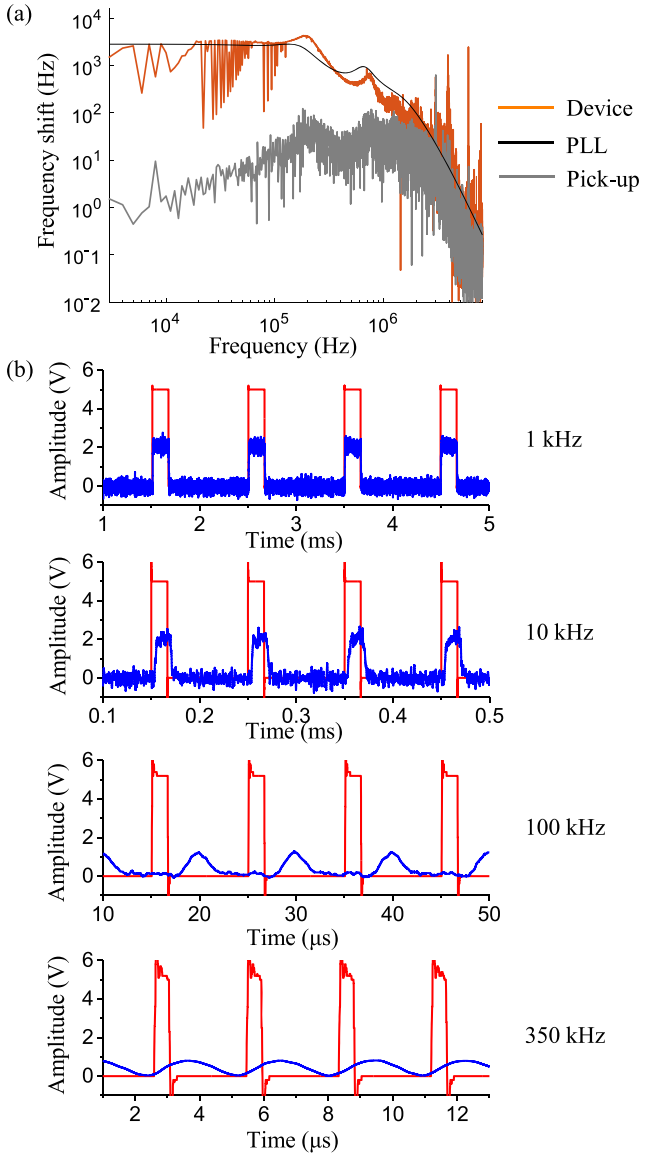

Figure 5. (a) Detection bandwidth of the device measured with PLL. Orange curve: experimental detection bandwidth of the device. Black curve: target transfer function of the PLL with a cutoff frequency at ~1 MHz. Gray: pickup signal from the PLL system measured in the absence of the QCL radiation. (b) Recovering pulse signals at different frequencies from 1 kHz up to 350 kHz by the device with PLL. Red: input pulse signal used to modulate THz radiation. Blue: output signal from the device.

nanolaser-based strain-engineered Ge beams,[29] where THz radiation can be used to control near-infrared wavelengths.

■ ASSOCIATED CONTENT

Supporting Information

The Supporting Information is available free of charge at https://pubs.acs.org/doi/10.1021/acsphotonics.2c00227.

(A) Optomechanical setup; (B) design and fabrication; (C) optical characterization; (D) mechanical characterization and calibration; (E) estimation of absorbed power on nanobeam; (F) temperature−frequency coefficient; (G) estimation of dielectric force; (H) thermal diffusion time on nanobeam; (I) power-dependent measurements of the device with a PLL system; (J) supplementary spectra of device A measured with various QCL power; (K) effects of electrodes on dogbone's THz response (PDF)

■ AUTHOR INFORMATION

Corresponding Authors

Jiawen Liu − *Laboratoire de Physique de l'Ecole Normale Supérieure, ENS, Université PSL, CNRS, Sorbonne Université, Université Paris Cité, F-75005 Paris, France;* orcid.org/0000-0002-1733-3501; Email: jiawen.liu@phys.ens.fr

Yanko Todorov − *Laboratoire de Physique de l'Ecole Normale Supérieure, ENS, Université PSL, CNRS, Sorbonne Université, Université Paris Cité, F-75005 Paris, France;* orcid.org/0000-0002-2359-1611; Email: yanko.todorov@phys.ens.fr

Authors

Baptiste Chomet − *Laboratoire de Physique de l'Ecole Normale Supérieure, ENS, Université PSL, CNRS, Sorbonne Université, Université Paris Cité, F-75005 Paris, France*

Paolo Beoletto − *Laboratoire de Physique de l'Ecole Normale Supérieure, ENS, Université PSL, CNRS, Sorbonne Université, Université Paris Cité, F-75005 Paris, France*

Djamal Gacemi − *Laboratoire de Physique de l'Ecole Normale Supérieure, ENS, Université PSL, CNRS, Sorbonne Université, Université Paris Cité, F-75005 Paris, France*

Konstantinos Pantzas − *Centre de Nanosciences et de Nanotechnologies (C2N), CNRS−Université Paris-Sud/Paris-Saclay, Palaiseau 91120, France;* orcid.org/0000-0002-2297-3247

Grégoire Beaudoin − *Centre de Nanosciences et de Nanotechnologies (C2N), CNRS−Université Paris-Sud/Paris-Saclay, Palaiseau 91120, France*

Isabelle Sagnes − *Centre de Nanosciences et de Nanotechnologies (C2N), CNRS−Université Paris-Sud/Paris-Saclay, Palaiseau 91120, France*

Angela Vasanelli − *Laboratoire de Physique de l'Ecole Normale Supérieure, ENS, Université PSL, CNRS, Sorbonne Université, Université Paris Cité, F-75005 Paris, France*

Carlo Sirtori − *Laboratoire de Physique de l'Ecole Normale Supérieure, ENS, Université PSL, CNRS, Sorbonne Université, Université Paris Cité, F-75005 Paris, France*

Complete contact information is available at: https://pubs.acs.org/10.1021/acsphotonics.2c00227

Funding

ANR-18-CE24-0025 Project TIGER and the ENS-Thales Chair.

Notes

The authors declare no competing financial interest.

■ ACKNOWLEDGMENTS

We acknowledge the technical support for clean room fabrication from Michael Rosticher, Pascal Filloux, Stéphan Suffit, Rémi Duhamel, and José Palomo. We also acknowledge the support from french Renatech network.

■ REFERENCES

(1) Ashkin, A. Optical Trapping and Manipulation of Neutral Particles Using Lasers. *Proc. Natl. Acad. Sci. U. S. A.* **1997**, *94* (10), 4853−4860.

(2) Pethig, R. Review Article—Dielectrophoresis: Status of the Theory, Technology, and Applications. *Biomicrofluidics* **2010**, *4* (2), 022811.

(3) Unterreithmeier, Q. P.; Weig, E. M.; Kotthaus, J. P. Universal Transduction Scheme for Nanomechanical Systems Based on Dielectric Forces. *Nature* **2009**, *458* (7241), 1001−1004.
(4) Aspelmeyer, M.; Kippenberg, T. J.; Marquardt, F. Cavity Optomechanics. *Rev. Mod. Phys.* **2014**, *86* (4), 1391−1452.
(5) Arcizet, O.; Cohadon, P. F.; Briant, T.; Pinard, M.; Heidmann, A. Radiation-Pressure Cooling and Optomechanical Instability of a Micromirror. *Nature* **2006**, *444* (7115), 71−74.
(6) Masmanidis, S. C.; Karabalin, R. B.; De Vlaminck, I.; Borghs, G.; Freeman, M. R.; Roukes, M. L. Multifunctional Nanomechanical Systems via Tunably Coupled Piezoelectric Actuation. *Science* **2007**, *317* (5839), 780−783.
(7) Belacel, C.; Todorov, Y.; Barbieri, S.; Gacemi, D.; Favero, I.; Sirtori, C. Optomechanical Terahertz Detection with Single Meta-Atom Resonator. *Nat. Commun.* **2017**, *8* (1), 2−9.
(8) Calabrese, A.; Gacemi, D.; Jeannin, M.; Suffit, S.; Vasanelli, A.; Sirtori, C.; Todorov, Y. Coulomb Forces in THz Electromechanical Meta-Atoms. *Nanophotonics* **2019**, *8* (12), 2269−2277.
(9) Akyildiz, I. F.; Jornet, J. M.; Han, C. Terahertz Band: Next Frontier for Wireless Communications. *Phys. Commun.* **2014**, *12*, 16−32.
(10) Nagatsuma, T.; Ducournau, G.; Renaud, C. C. Advances in Terahertz Communications Accelerated by Photonics. *Nat. Photonics 2016 106* **2016**, *10* (6), 371−379.
(11) Tonouchi, M. Cutting-Edge Terahertz Technology. *Nat. Photonics 2007 12* **2007**, *1* (2), 97−105.
(12) Lewis, R. A. A Review of Terahertz Detectors. *J. Phys. D. Appl. Phys.* **2019**, *52* (43), 433001.
(13) Alves, F.; Grbovic, D.; Kearney, B.; Lavrik, N. V.; Karunasiri, G. Bi-Material Terahertz Sensors Using Metamaterial Structures. *Opt. Express* **2013**, *21* (11), 13256.
(14) Zhang, Y.; Hosono, S.; Nagai, N.; Song, S.-H.; Hirakawa, K. Fast and Sensitive Bolometric Terahertz Detection at Room Temperature through Thermomechanical Transduction. *J. Appl. Phys.* **2019**, *125* (15), 151602.
(15) Faist, J.; Capasso, F.; Sivco, D. L.; Sirtori, C.; Hutchinson, A. L.; Cho, A. Y. Quantum Cascade Laser. *Science (80-.)* **1994**, *264* (5158), 553−556.
(16) Cleland, A. N.; Roukes, M. L. Noise Processes in Nanomechanical Resonators. *J. Appl. Phys.* **2002**, *92* (5), 2758−2769.
(17) Chomet, B.; Gacemi, D.; Vasanelli, A.; Sirtori, C.; Todorov, Y. Optomechanical Temporal Sampling of Terahertz Signals. *Appl. Phys. Lett.* **2021**, *119* (18), 181103.
(18) Fick, A. V. On Liquid Diffusion. *London, Edinburgh, Dublin Philos. Mag. J. Sci.* **1855**, *10* (63), 30−39.
(19) Landau, L. D.; Lifshitz, E. M. *Course of Theoretical Physics: Mechanics*; Butterworth-Heinemann: Oxford, 1982.
(20) Zhang, X. C.; Myers, E. B.; Sader, J. E.; Roukes, M. L. Nanomechanical Torsional Resonators for Frequency-Shift Infrared Thermal Sensing. *Nano Lett.* **2013**, *13* (4), 1528−1534.
(21) Zhang, Y.; Watanabe, Y.; Hosono, S.; Nagai, N.; Hirakawa, K. Room Temperature, Very Sensitive Thermometer Using a Doubly Clamped Microelectromechanical Beam Resonator for Bolometer Applications. *Appl. Phys. Lett.* **2016**, *108* (16), 163503.
(22) Zhang, Y.; Kondo, R.; Qiu, B.; Liu, X.; Hirakawa, K. Giant Enhancement in the Thermal Responsivity of Microelectromechanical Resonators by Internal Mode Coupling. *Phys. Rev. Appl.* **2020**, *14* (1), 14019.
(23) Jeannin, M.; Bonazzi, T.; Gacemi, D.; Vasanelli, A.; Li, L.; Davies, A. G.; Linfield, E.; Sirtori, C.; Todorov, Y. Absorption Engineering in an Ultrasubwavelength Quantum System. *Nano Lett.* **2020**, *20* (6), 4430−4436.
(24) Benz, A.; Campione, S.; Liu, S.; Montaño, I.; Klem, J. F.; Allerman, A.; Wendt, J. R.; Sinclair, M. B.; Capolino, F.; Brener, I. Strong Coupling in the Sub-Wavelength Limit Using Metamaterial Nanocavities. *Nat. Commun.* **2013**, *4* (1), 2882.
(25) Cadeddu, D.; Braakman, F. R.; Tütüncüoglu, G.; Matteini, F.; Rüffer, D.; Fontcuberta i Morral, A.; Poggio, M. Time-Resolved Nonlinear Coupling between Orthogonal Flexural Modes of a Pristine GaAs Nanowire. *Nano Lett.* **2016**, *16* (2), 926−931.
(26) Foster, A. P.; Maguire, J. K.; Bradley, J. P.; Lyons, T. P.; Krysa, A. B.; Fox, A. M.; Skolnick, M. S.; Wilson, L. R. Tuning Nonlinear Mechanical Mode Coupling in GaAs Nanowires Using Cross-Section Morphology Control. *Nano Lett.* **2016**, *16* (12), 7414−7420.
(27) Almog, R.; Zaitsev, S.; Shtempluck, O.; Buks, E. Noise Squeezing in a Nanomechanical Duffing Resonator. *Phys. Rev. Lett.* **2007**, *98* (7), 078103.
(28) Huber, J. S.; Rastelli, G.; Seitner, M. J.; Kölbl, J.; Belzig, W.; Dykman, M. I.; Weig, E. M. Spectral Evidence of Squeezing of a Weakly Damped Driven Nanomechanical Mode. *Phys. Rev. X* **2020**, *10* (2), 021066.
(29) Bao, S.; Kim, D.; Onwukaeme, C.; Gupta, S.; Saraswat, K.; Lee, K. H.; Kim, Y.; Min, D.; Jung, Y.; Qiu, H.; Wang, H.; Fitzgerald, E. A.; Tan, C. S.; Nam, D. Low-Threshold Optically Pumped Lasing in Highly Strained Germanium Nanowires. *Nat. Commun. 2017 81* **2017**, *8* (1), 1−7.

https://doi.org/10.1021/acsphotonics.2c00227
ACS Photonics XXXX, XXX, XXX−XXX